Electronic Supplementary Material (ESI) for Journal of Materials Chemistry A.

Supplementary Information

Acoustotemplating: Rapid Synthesis of Freestanding Quasi-2D MOF/Graphene Oxide Heterostructures for Supercapacitor Applications

Yemima Ehrnst,[†] Heba Ahmed,[†] Robert Komljenovic,[†] Emily Massahud,[†] Nick A. Shepelin,[‡,¶] Peter C. Sherrell,[¶] Amanda V. Ellis, [¶] Amgad R. Rezk,[*,†] and Leslie Y. Yeo[†]

† *Micro/Nanophysics Research Laboratory, School of Engineering, RMIT University, Melbourne, VIC 3001, Australia*

‡ *Laboratory for Multiscale Materials Experiments, Paul Scherrer Institut, CH-5232 Villigen, Switzerland*

¶ *Department of Chemical Engineering, The University of Melbourne, Parkville, Victoria 3010, Australia*

Email: amgad.rezk@rmit.edu.au

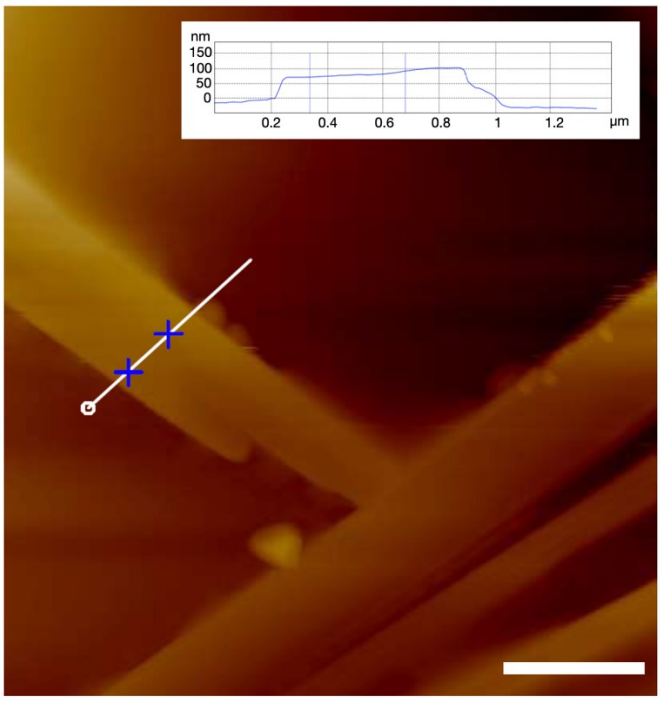

Figure S1 Atomic force microscopy image of a typical q-2D-MOF; the scale bar represents a length of 1 µm. The inset shows the height profile of the MOF.

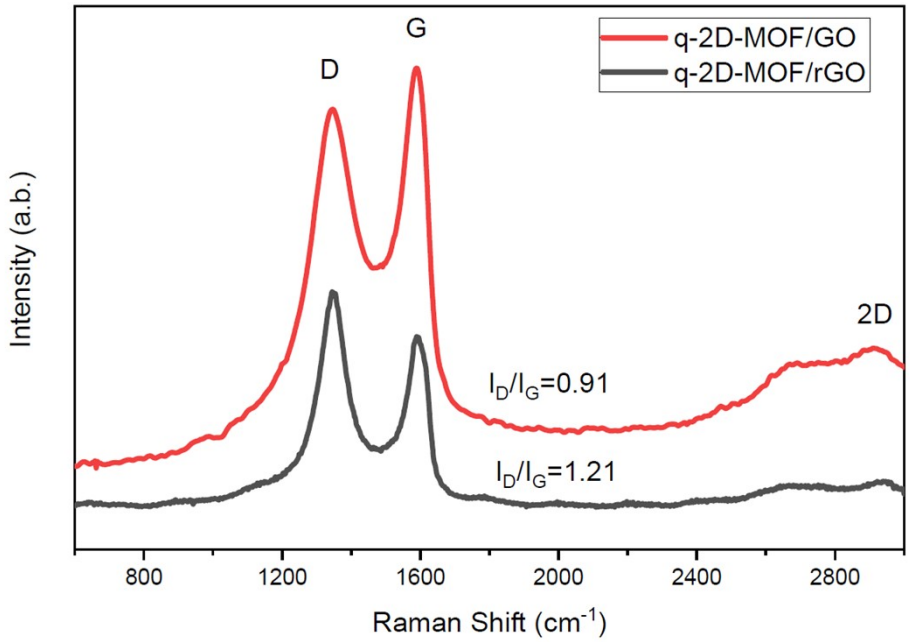

Figure S2 Raman spectra of the q-2D-MOF/GO and q-2D-MOF/rGO composites showing the calculated relative intensities of the D and G bands. The ratio of the intensities between both bands, I_D/I_G, for the unreduced sample is 0.91, which increases to 1.21 for the reduced sample, indicating an increase in the number of smaller graphene domains in the latter.

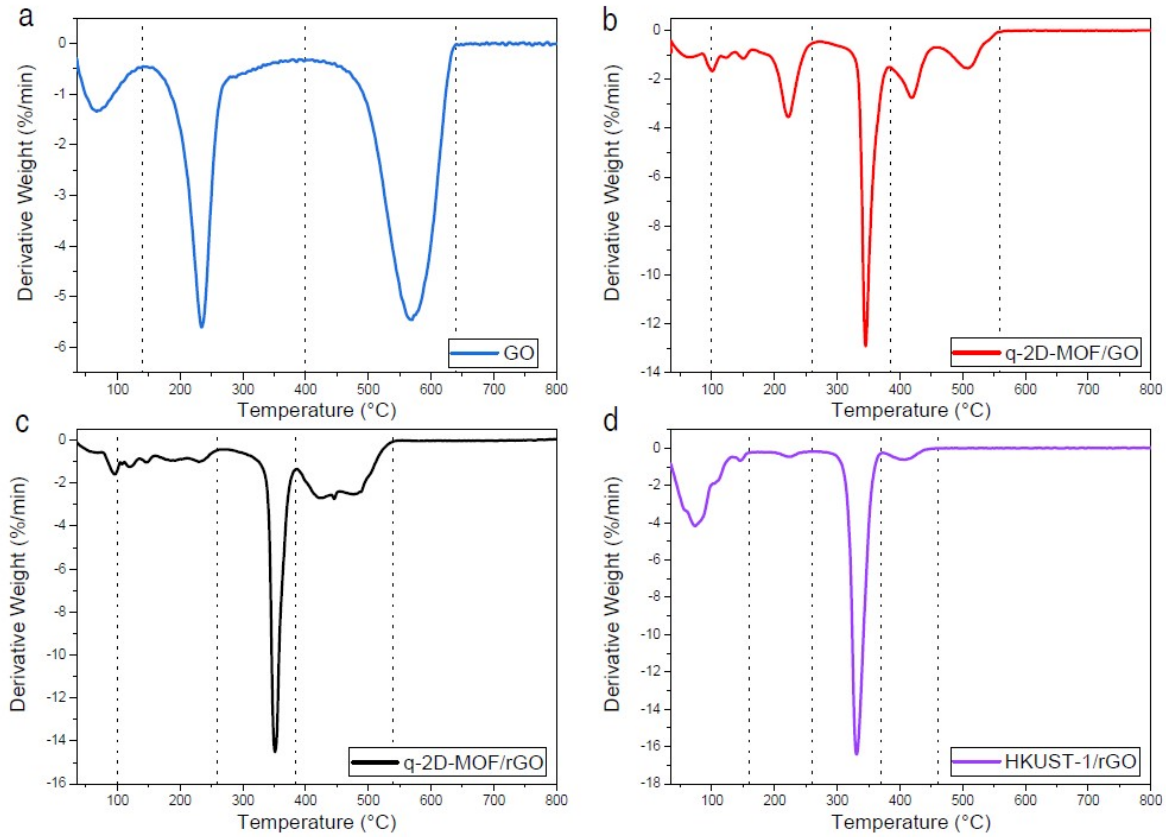

Figure S3 Differential thermal analysis (DTA) of (a) GO, (b) q-2D-MOF/GO, (c) q-2D-MOF /rGO, and, (d) HKUST-1/rGO. The dotted lines reference the temperature regions of interest that are discussed in the manuscript. The shift of the second GO peak to the right is indicative of the reduction of GO in the sample.

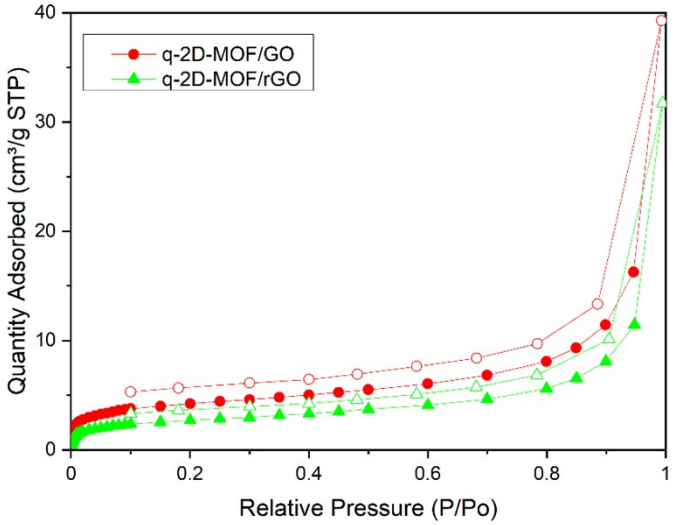

Figure S4 N_2 absorption–desorption isotherms for the q-2D-MOF/GO and q-2D-MOF/rGO composites, yielding BET surface areas of 15.1 and 9.6 $m^2 g^{-1}$, respectively. The low surface area values are not uncommon for 2D-MOFs with highly exposed metal sites and large lateral-area-to-

volume ratios,[1-3] and are compounded by the formation of meso- and macro-pores as a result of the incorporation of GO and bound water molecules.

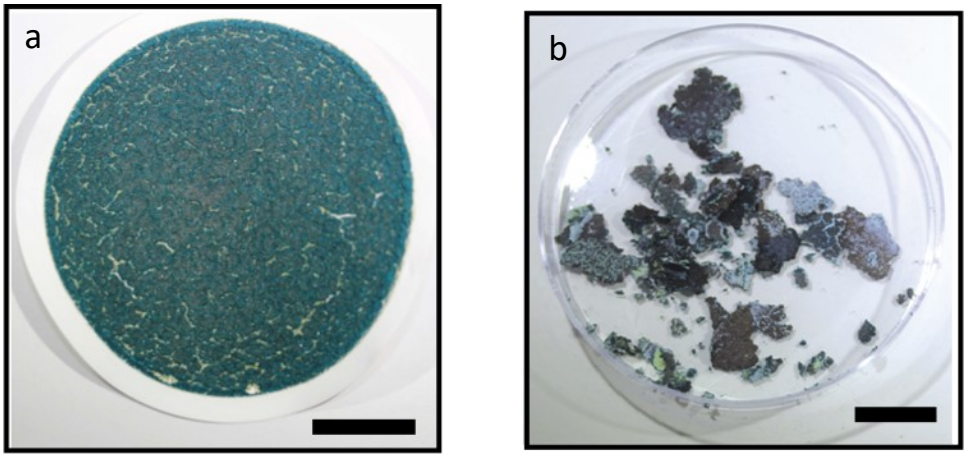

Figure S5 Control HKUST-1/GO synthesized without the acoustic excitation, (a) before, and, (b) after reduction via UV/L-AA, showing its brittle nature, with obvious crumbling and cracking of the film. The scale bars denote a length of approximately 1 cm.

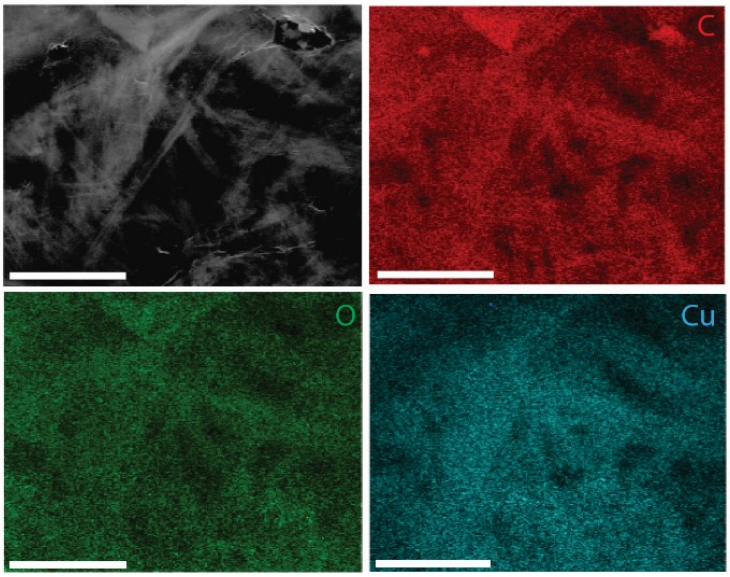

Figure S6 Scanning electron microscopy (SEM) image of the q-2D-MOF /rGO sample and corresponding regions showing the carbon, oxygen and copper elements from the energy-dispersive x-ray spectroscopy (EDX) analysis; the scale bars denote a length of 5 µm.

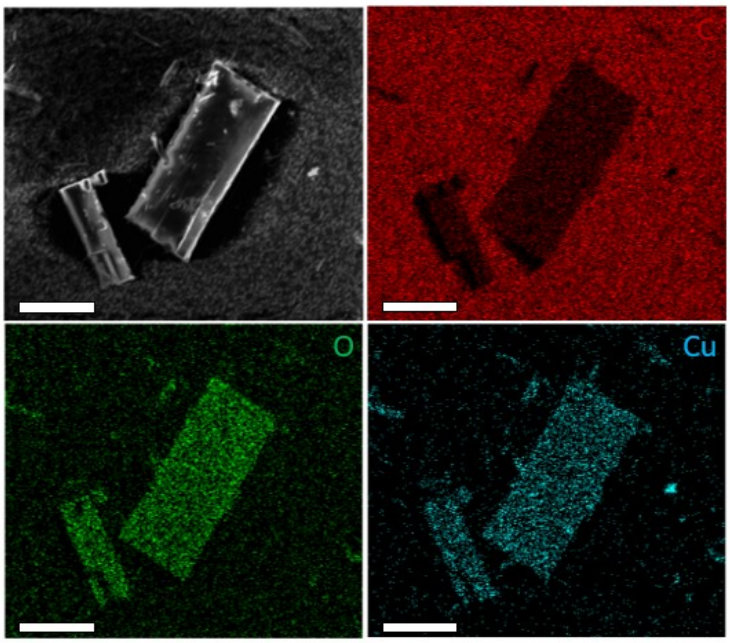

Figure S7 SEM image of the control HKUST-1/rGO sample and corresponding regions showing the carbon, oxygen and copper elements from the EDX analysis, in which we observe the lack of homogeneity across the sample; the scale bars denote a length of 10 µm.

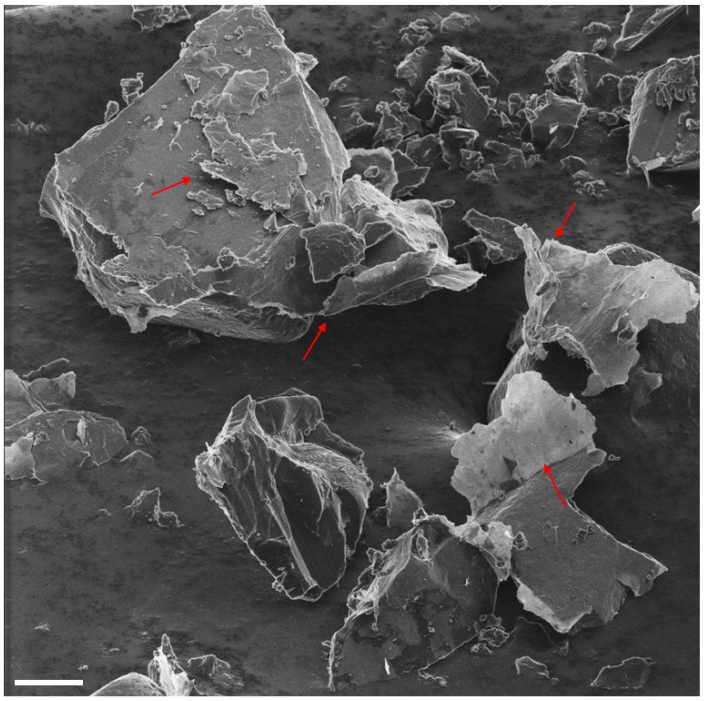

Figure S8 Representative helium ion microscopy (HIM) image of the HKUST-1/GO composite, showing the 3D Cu-BTC (Basolite or HKUST-1) crystals sporadically covered by localised GO sheets (as indicated by the arrows). The scale bar represents denote a length of 10 µm.

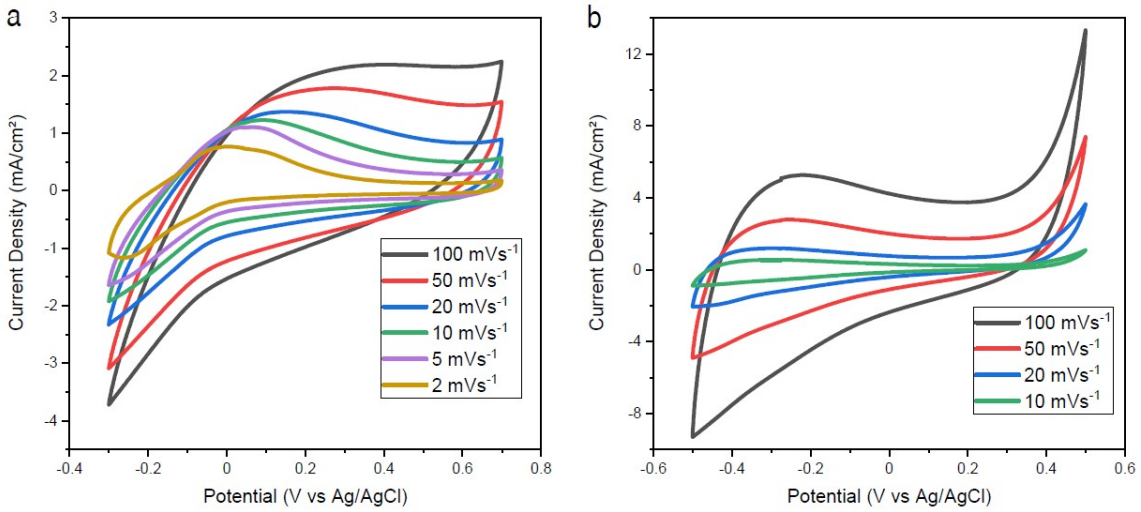

Figure S9 Cyclic voltammetry (CV) curves for the q-2D-MOF /rGO composite in (a) 1 M Na_2SO_4, and, (b) 6 M KOH. Different voltage windows were used to obtain the optimal curve responses from which the specific areal and gravimetric capacitances were calculated and presented in Table S3. The poor area to scan-rate relationship depicted in (b) reflects the incompatibility between the material and the electrolyte.

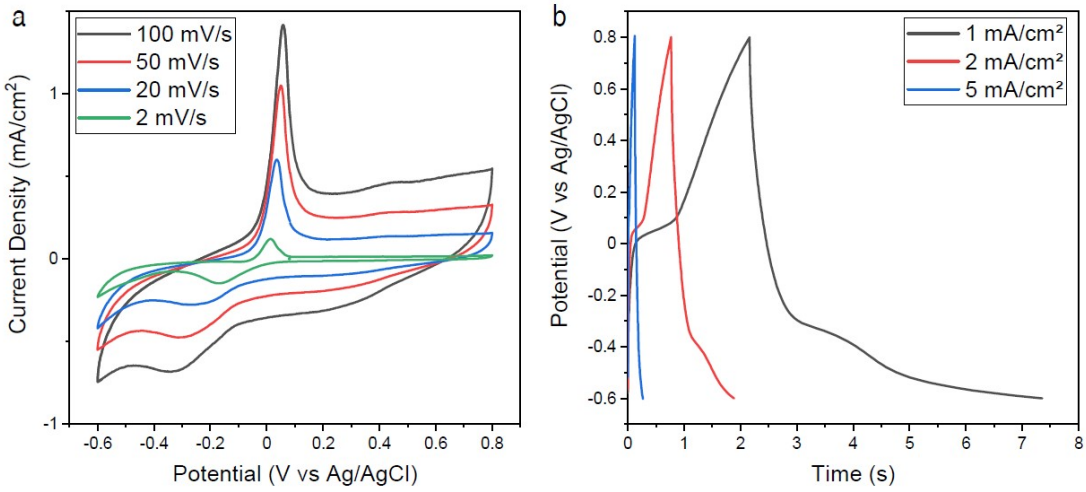

Figure S10 (a) Cyclic voltammetry (CV) and (b) galvanic charge–discharge (GCD) curves at various current various densities for HKUST-1/rGO in 1 M Na_2SO_4. The specific areal and gravimetric capacitances calculated from these results are presented in Tables S5.

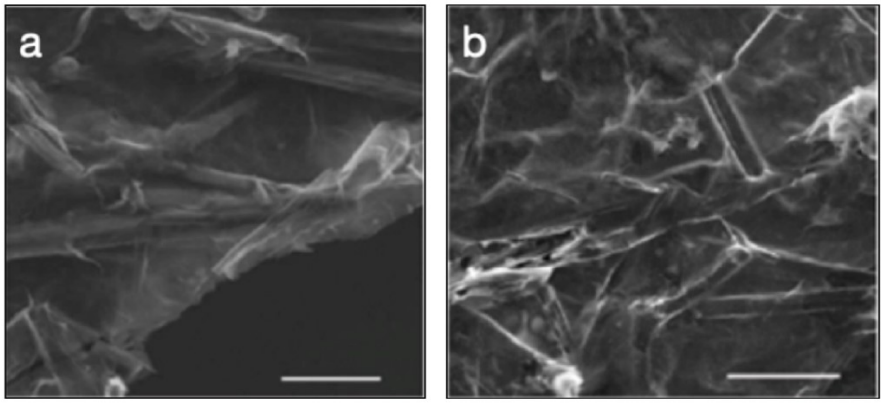

Figure S11 (a,b) SEM images of the q-2D-MOF/rGO composite, (a) before and (b) after 1000 cycles, indicating that the q-2D-MOFs remain intact and coordinated to the GO sheets; the scale bars denote lengths of 25 µm.

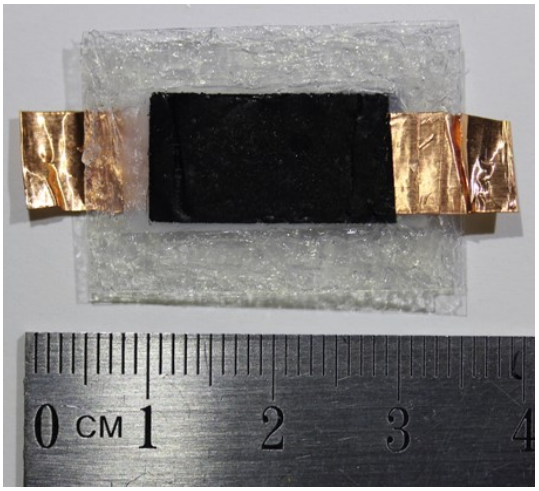

Figure S12 Image of the fabricated flexible solid-state supercapacitor device with copper foil tongues.

Table S1 FTIR peak assignment for q-2D-MOF/rGO for all positions highlighted in Fig 3c. Notes are provided for clarification as appropriate.

Peak Position (cm^{-1})	Assignment	Note
690	Cu–O stretching	
747	Cu–O stretching	
890	C–H bending	Aromatic meta-bond substitution; absent from q-2D-MOF/GO and q-2D-MOF/rGO spectra due to π- π interactions.
1040	C–O stretching	Alcohol
1114	C–O–Cu stretching	Characteristic of Cu-BTC
1180	C–O stretching	Ester
1235	C–O–C stretching	
1362	O–H bending	Present in both the GO sheets and the H_3BTC linker from carboxylic group
~1550	C=C stretching (symmetric)	
1617	C=C (asymmetric aromatic)	Present in both the GO sheets and the H_3BTC linker
1704	COO– stretching (asymmetric)	Specifically C=O
~3150	O–H stretching	Intercalated H_2O (3300 cm^{-1} specifically; intramolecular OH groups weakly present in q-2D-MOF/rGO)

Table S2 Quantification of bonds based on the area under the peak for the deconvoluted XPS C 1s spectra. An increase in C–C bonds is observed as some oxygen groups are reduced and the sp^2 network restored. The percentage increase in O–C=O bonds can be attributed to the bonds within the organic linker remaining unchanged after reduction and therefore accounts for a larger contribution to the q-2D-MOF/rGO C 1s spectra.

q-2D-MOF/rGO C 1s	
C–C	65.9%
C–OH	10.4%
C–O–C	12.2%
C=O	**5.4%**
O–C=O	6.2%

HKUST-1/rGO C 1s	
C–C	49.1%
C–OH	14.6%
C–O–C	8.8%
C=O	**22.0%**
O–C=O	5.5%

Table S3 Capacitance values for q-2D-MOF/rGO in neutral and basic electrolytes.

1M Na_2SO_4 Electrolyte		
Scan Rate (mVs^{-1})	Areal Capacitance (mF/cm^2)	Specific Capacitance (F/g)
100	15.33	9.85
50	24.77	15.92
20	43.48	27.94
10	66.85	42.96
5	100.60	64.65
2	154.90	99.54
6M KOH Electrolyte		
Scan Rate (mVs^{-1})	Areal Capacitance (mF/cm^2)	Specific Capacitance (F/g)
100	48.88	31.41
50	43.47	27.93
20	47.26	30.37
10	40.23	25.85

Table S4 Capacitance values for q-2D-MOF/rGO derived from the GCD measurements.

Current Density		Capacitance	
(mA/cm²)	(A/g)	(mF/cm²)	(F/g)
1	0.73	401.4	292.5
2	1.46	227.0	165.4
5	3.66	139.7	101.8

Table S5 Capacitance values for HKUST-1/rGO derived from the CV and GCD measurements.

CV		GCD	
(mV/s)	(F/g)	(mA/cm²)	(mF/cm²)
100	2.4	1	3.5
50	3.2	2	1.6
20	4.6	5	0.5
2	12.9		

Table S6 Equivalent circuit parameters associated with the fitted Nyquist plots.

q-2D-MOF/rGO before 1000 cycles	
Parameter (units)	**Value**
R1 (Ω)	-1.213
R2 (Ω)	68.62
C_{dl} ($Fs^{1/a}$)	15.06×10^{-6}
a	0.5462
W ($\Omega\ s^{-1/2}$)	998
q-2D-MOF/rGO after 1000 cycles	
R1 (Ω)	-5.551
R2 (Ω)	64.75
C_{dl} ($Fs^{1/a}$)	22.23×10^{-6}
a	0.5044
W ($\Omega\ s^{-1/2}$)	1047

Calculation of Specific Areal and Gravimetric Capacitances

The specific areal capacitance C_a (mF/cm^2) and gravimetric capacitance C_s (F/g) was calculated from the CV curves using the following relationships:[1]

$$C_a = \frac{\int_{Va}^{Vc} I(V)dV}{av\Delta V} \quad \text{(S1)}$$

$$C_s = \frac{\int_{Va}^{Vc} I(V)dV}{mv\Delta V} \quad \text{(S2)}$$

where $\int_{Va}^{Vc} I(V)dV$ is the integral of the CV curve, a is the area of active material (cm^2), m is the mass of the active material (g), v is the scan rate (Vs^{-1}) and $\Delta V = V_c - V_a$ is the potential difference (V).

Alternatively, the specific areal capacitance and gravimetric capacitances can be obtained from the GCD curves using the following relationships:[4]

$$C_a = \frac{I\Delta t}{a\Delta V} \quad \text{(S3)}$$

$$C_s = \frac{I\Delta t}{m\Delta V} \quad \text{(S4)}$$

where I is the applied current (A), Δt is the discharge time (s), and ΔV is the potential window accounting for the IR drop (V).

For a symmetrical 2-electrode device, the specific gravimetric capacitance (F/g) was calculated from[5]

$$C_s = \frac{4\int_{Va}^{Vc} I(V)dV}{mv\Delta V} \quad \text{(S5)}$$

References

1. Beka, L. G.; Bu, X.; Li, X.; Wang, X.; Han, C.; Liu, W. A 2D Metal–Organic Framework/Reduced Graphene Oxide Heterostructure for Supercapacitor Application. *RSC Adv.* **2019**, 9, 36123–36135.
2. Wang, M.; Dong, R.; Feng, X. Two-Dimensional Conjugated Metal–Organic Frameworks (2D c-MOFs): Chemistry and Function for MOFtronics. *Chem. Soc. Rev.* **2021**, 50, 2764–2793.
3. Singh, M.K.; Gupta, A.K.; Krishnan, S.; Guha, N.; Marimuthu, S.; Rai, D.K. A New Hierarchically Porous Cu-MOF Composited with rGO as an Efficient Hybrid Supercapacitor Electrode Material. *J. Energy Storage* **2021**, 43, 103301.
4. Van Ngo, T.; Moussa, M.; Tung, T.T.; Coghlan, C.; Losic, D. Hybridisation of MOFs and Graphene; A new strategy for the synthesis of porous 3D carbon composites for high performing supercapacitors. *Electrochim. Acta* **2020**, 339, 135104.
5. Moussa, M.; El-Kady, M.F.; Zhao, Z.; Majewski, P.; Ma, J. Recent progress and performance evaluation for polyaniline/graphene nanocomposites as supercapacitor electrodes. *Nanotechnology* **2016**, 27, 442001.